ISSN:1991-8178

Australian Journal of Basic and Applied Sciences

Journal home page: www.ajbasweb.com

Efficient Automated Segmentation and Lossless Compression of Fluoroscopic Images

[1,2]Arif Sameh Arif, [1]Sarina Mansor, [3]Rajasvaran Logeswaran and [1]Hezerul Abdul Karim

[1]*Multimedia University, Faculty of Engineering, 63100 Cyberjaya, Selangor, Malaysia*
[2]*Middle Technical University, Institute of Administration Rassafa, Baghdad, Iraq.*
[3]*Asia Pacific University of Technology & Innovation, 57000 Kuala Lumpur, Malaysia.*

ARTICLE INFO

Article history:
Received 12 November 2014
Received in revised form 26 December 2014
Accepted 29 January 2015
Available online 10 February 2015

Keywords:
Fluoroscopy medical images ROI Lossless image compression Run-length Coding Huffman Coding Correlation.

ABSTRACT

Systematic procedures for data storage and retrieval are obligatory to the fluoroscopy and other conventional diagnostic imaging devices in which they produce a large number of medical images. This paper proposes and efficient method for lossless compression of fluoroscopic images. There are two components in this paper; segmentation and compression. For the rectangular inside the image, a scheme on automated segmentation and extraction was developed. The development includes the derivation of the general equation with the purpose of extracting the rectangle, then perform lossless compression of targeted parts within fluoroscopy images. In this paper, the cropped region of interest (ROI) are pharynx and esophagus whereby it goes through the extraction and compression process. To improve the compression efficiency, the correlation and combination of Run Length and Huffman coding are used in the extraction and compression stage. The experimental results of the proposed method have shown that the achieved compression ratio show has improved by 400% when compared to traditional techniques.

To Cite This Article: Arif Sameh Arif, Sarina Mansor, Rajasvaran Logeswaran and Hezerul Abdul Karim., Efficient Automated Segmentation and Lossless Compression of Fluoroscopic Images. ***Aust. J. Basic & Appl. Sci.,*** *9(5): 220-228, 2015*

INTRODUCTION

Medical imaging is the key to today's diagnoses and treatment in the field of medicine. Different techniques allow for non-invasively examining the insides of a patient and minimize recovery time, this reality encourages the doctors to rely on medical images.Hospitals and medical centers have seen a tremendous increase in the use of diagnostic imaging that produce a large series of images in each examination. This has led to increasing loads and costs of processing, transmission, handling and storage. Although technologies for these have increased rapidly, medical institutions are struggling to cope with the sheer volume of new images generated daily.

It is very difficult for hospitals to manage the storage facilities for these digital images. Moreover, such high amounts of data demands high-end networks, especially in telemedicine. This is a very significant issue owing to the limitations of the transmission media in information and communication technology, especially in the less developed, rural and remote areas. Image compression is useful in reducing the storage and transmission bandwidth requirements of medical images (Bairagi, V., A. Sapkal, 2012).

The defacto technique for medical images is lossless compression, where prolixity in the data is removed without any loss of reliability, and the images can be restored to its original state upon decompression (Kumar, N., C. Kamargaonkar, 2013; Ukrit, M., 2011). However, many researchers nowadays are attempting lossy compression of medical images as it enables better performance in terms of reduced final file size, although this comes at the cost of losing some level of accuracy. To legitimize the applicability of lossy compression in medical diagnosis, work such as in (Choong, M., 2006) have pledged to show that due to the defects of the imaging equipment which inherently introduces noise into the images, controlled lossy compressed images tend to be preferred by medical practitioners in a double-blind experiment where the experts were asked to indicate which images they considered as more accurate.

Background:

Medical images can be classified into two main modes: a single or limited number of independent images per examination as in the case of X-ray, and

Corresponding Author: Sarina Mansor, Multimedia University, Faculty of Engineering, 63100 Cyberjaya, Selangor, Malaysia

sequential images that are produced by the Computed Tomography (CT), Magnetic Resonance Imaging (MRI), and Fluoroscopy imaging modalities. Fluoroscopy is a particular kind of X-ray that provides series of X-ray images of a patient's organ structure in real-time. It is used in many types of checkups and procedures, such as cardiac catheterization, Percutaneous Nephrostomy (PCN), Barium Swallow and others. Fluoroscopy images are used to provide real-time interpretive data to surgeons during an operation. However, these images can be very tricky for a computer to interpret as each pixel represents the entire path of tissue, air, and bone travelled by the X-ray from the source to the detector plate (Mei-Yen, C., 2007; Russakoff, D., 2002).

Segmentation is a process that splits an image into objects or its shape parts. Relying on the quality and noise present in the image, some segmentation techniques may require image pre-processing prior to the segmentation method; others may need post-processing operations exclude the effects of a possible over segmentation (Novoa, F., 2011).

Region of interest (ROI) usually means the significative and significant regions in the images. The use of ROI can avert the processing of irreverent image points and expedite the processing. Extraction of ROI from images is a significant topic in the image processing area, especially in medical image processing. During image transmission for telemedicine purposes, there are regions that are required to be transmitted first or at a higher priority. In transformation-based ROI coding methods, the coefficients associated with the ROI are transferred ahead of those associated with the background. Therefore, when an image is coded with an emphasis on ROI, it is necessary to identify the coefficients required for the reconstruction of the ROI. Thus, an ROI mask is introduced to indicate which coefficients have to be transmitted exactly, in order for the receiver to reconstruct the ROI (Doukas, C., I. Maglogiannis, 2007; Zhang, Q., H. Xiao, 2008).

Correlation coefficient (CC) is one of the most common symmetry measures, and it helps highlight variations. CC measures the symmetry existing between two images, and it has been used to elucidate the quality of a least squares fitting of the sequence of images (V˘aduva, C., 2013).

Huffman coding is a variable length coding that specifies longer codes to symbols with low probabilities and short bit code to symbols with higher possibilities. This coding scheme is effective in compressing differential data (Song, T., T. Shimamoto, 2007). The Run-length coding is one of the most well-known and simplest methods applied to encode iterative data or code pattern in a single code (Nu´n˜ez, J., S. Jones, 2003).

The combination of the two efficient compression methods, Run-length and Huffman coding, was proposed to decrease the data volume, pattern delivery time, and economize power in scan applications (Norani, M., M. Tehranipour, 2005). In medical images, the combination of Run-length and Huffman coding was implemented on X-ray angiograms, and MRI images to fulfil maximum compression (Sunder, R., 2005). The same combination of Run-length and Huffman coding was executed for color images after quantization and threshoding, enabling the Discrete Wavelet Transform (DWT) coefficients to gain a better result in (Setia, V., V. Kumar, 2012).

In our recent work, we implemented lossless compression of Fluoroscopy medical images using correlation and Huffman coding (Arif, A., 2012). The proposed method achieved an average compression ratio of 7.97. We extended the work to include the combination of Huffman and Run-length coding. Specifically, we proposed a new framework for lossless medical image compression based on classification of the images by correlation and coding the differences between the sequential images using the combination of Run-length and Huffman coding. The extended method attained an improved compression ratio of 11.41 (Arif, A., 2012). We then extended the work by extracting the ROI from each image, calculating the CC to examine the similarity between them, finding the differences between the two ROIs, and then only applying the Run-length and Huffman coding (R. Huff-Seg.) combination method to gain further improvement in compression. The extended method attained significantly improved compression ratio of 29.73 (Sameh, A., 2013).

In this paper, we extend the work further by introducing automatic extracting for the Region of Coding (ROC) of the rectangle inside the image and cropping the extracted ROI from each image, calculating the CC to examine the level of similarity between them, finding the differences between the two cropped ROIs, and then only applying the Run-length and Huffman coding (R. Huff-Crop.) combination method to gain further improvement in compression performance. To the best of our knowledge, there are no other published works employing this technique in the context of medical image compression.

Region of Interest and Correlation:

Identifying and extracting a precise ROI is the fundamental step before coding and compressing the image data for effective transmission or storage. By using various spatial regions and identifying the ROI of the image, it is possible to compress it into various levels of reconstruction qualification. Images can be categorized into three regions: (1) Primary region of interest (PROI), (2) Secondary region of interest (SROI) and (3) background (Akhtar, P., 2007). This way, one could precisely maintain the features necessary for medical diagnosis or scientific measurement, while achieving higher overall

compression by allowing degradation of data in the inconsequential regions (Kumar, R., 2008).

The correlation is specified by the variance and co-variance, where the variance is measured for a dimension with itself, while the covariance is measured between two dimensions. The formulae for the calculation of variance (Var) and co-variance (Cov) are given as follows (Javed, M., M. Khan, 2008; Ramesh, S., 2010):

$$Var(X) = \frac{\sum_{i-1}^{n}(X_i - X^b)}{n-1} \quad (1)$$

$$Var(Y) = \frac{\sum_{i-1}^{n}(Y_i - Y^b)}{n-1} \quad (2)$$

$$Cov(X,Y) = \frac{\sum_{i-1}^{n}(X_i - X^b)(Y_i - Y^b)}{n-1} \quad (3)$$

$$R_{XY} = \frac{Cov(X,Y)}{Var(X)Var(Y)} \quad (4)$$

where X^b and Y^b are the means of X and Y, respectively, and R is the correlation between X and Y.

To calculate the correspondence between the original image and the reconstructed image, the correlation coefficient (CC) is calculated as follows:

$$CC = \frac{\sum_s \sum_t [f(s,t) - \bar{f}(s,t)][w(x+s,y+t) - \bar{w}]}{\{\sum_s \sum_t [f(s,t) - \bar{f}(s,t)]^2 \sum_s \sum_t [w(x+s,y+t) - \bar{w}]^2\}^{1/2}} \quad (5)$$

where $x = \{0, 1, 2,\ldots, M\text{-}1\}$, $y = \{0, 1, 2,\ldots, N\text{-}1\}$, $\bar{w}$ is the average value of the pixels in w, $\bar{f}$ is the average value of f (intensity function) in the region coincident with the current location of w, the summations are taken over the coordinates common to both f and w, and $M \times N$ is the size of the original image. The CC is scaled in the range (-1 to 1), independent of scale changes in the amplitude of f and w (Bharti, P., 2009).

Methodology:

The proposed framework can be divided into three main stages: Classification, Segmentation and Encoding as shown in Fig. 1. The process is reversed to remodel the series of images upon decompression.

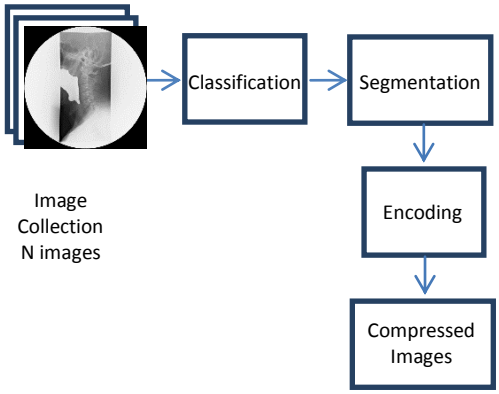

Fig. 1: Proposed framework.

A. Classification:

The morphology of the fluoroscopy images leads us to classify the images of each patient into groups, relying on the angle of view. So, the initial step in classification is to create a group, considering the first image as a reference and comparing the other images with it by calculating the CC. This step generates up to three groups for each patient. Duplicated images, including the ones in which the radiographer moves and/or the patient moves, are transferred to a shifted group. The pivotal part in esophagus fluoroscopy images is following the contrast agent (liquid) that is usually depicted in high intensity, sliding down the esophagus of the patient. Fig. 2 summarizes the stage.

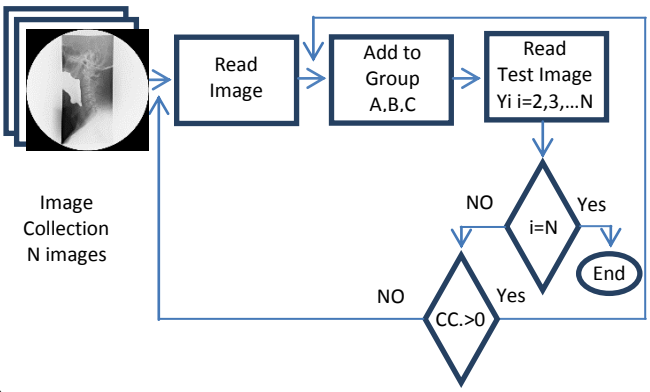

Fig. 2: Classification Stage.

B. Segmentation:

For this stage, we proposed an automated segmentation which is summarized as follows:

B-1Remove Image Background (black areas):

Depending on the shape of the fluoroscopy images, there are commonly four black corners in each image (see Fig. 3). By fixing the center of the image and measuring the distance from the center to the brink of the image, we can identify a circular area that comprises the actual data from the fluoroscopy device, leaving out the unused black area.

B-2 Automated Segmentation:

A general equation could be derived to extract the ROC region. In fluoroscopy images, as shown in Fig. 3., obviously there are fourcircular segments in each image that do not include any significant information and can be regarded background area. The significant information is contained within a rectangular ROC area. This area could be extracted through various means, including histogram analysis of the intensity difference between the rectangle and the circle segments. However, such a process often involves inaccurate manual intervention during identification of the accurate intensity value to extract the rectangle in each image.

As the shapes of the areas in question are relatively well-defined, a geometric solution is proposed. In this work, a new algorithm is introduced for the extraction of the rectangle (i.e., the ROC). This Rectangle-Clipping algorithm starts by using some known attributes of the circle (e.g., the coordinates of the center and radius *r*), calculates the size of the circular segment areas on the four sides (top, bottom, left and right)surrounding the rectangle and subtracts them from the whole circle area, as shown in Fig. 4. The relevant derivation steps are given below.

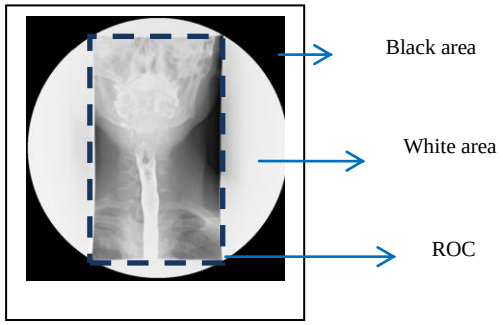

Fig. 3: Important areas in Fluoroscopy images.

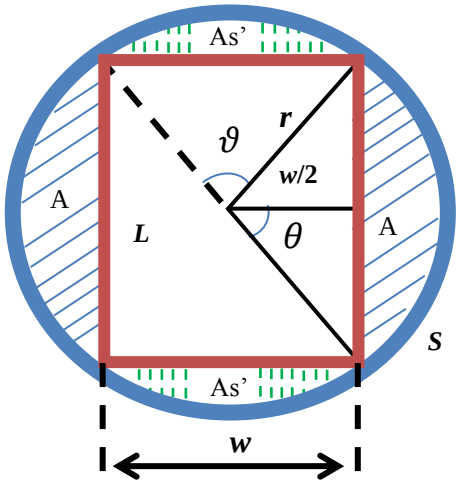

Fig. 4: The structure of Fluoroscopy images.

We can derive the general equation to calculate the area of the rectangle inside the circle from the equation of the area of the segment. Starting from the center of the image to calculate the width of the rectangle, as shown below:

Using trigonometry and the known attributes of the circle in Fig. 4,

$$Area\ of\ segment\ (As) = \frac{r^2}{2}(\theta - sin\,\theta) \quad (6)$$

$$Area\ of\ the\ circle\ (Ac) = \pi r^2 = \frac{\pi}{4}d^2 \quad (7)$$

and

$$cos\left(\frac{\theta}{2}\right) = \frac{\left(\frac{w}{2}\right)}{r} = \frac{\left(\frac{w}{2}\right)}{\left(\frac{d}{2}\right)} = \frac{w}{d} \quad (8)$$

Where d is the diameter of the circle =2r.
so,

$$\frac{\theta}{2} = cos^{-1}\left(\frac{w}{d}\right) \quad (9)$$

and consequently,

$$\theta = 2\cos^{-1}\left(\frac{w}{d}\right) \quad (10)$$

Therefore, substituting into Eq. (8), we get:

$$As = \frac{1}{2}r^2\left[2\,cos^{-1}\left(\frac{w}{d}\right) - sin\left(2\,cos^{-1}\left(\frac{w}{d}\right)\right)\right] \quad (11)$$

so,

$$2As = \frac{d^2}{4}\left[2\,cos^{-1}\left(\frac{w}{d}\right) - sin\left(2\,cos^{-1}\left(\frac{w}{d}\right)\right)\right] \quad (12)$$

Similarly, the area of the circle segments at the top and bottom of the rectangle (i.e., *As′*) can be calculated using the following equations:

$$sin\left(\frac{\vartheta}{2}\right) = \frac{\left(\frac{w}{2}\right)}{r} = \frac{\left(\frac{w}{2}\right)}{\left(\frac{d}{2}\right)} = \frac{w}{d} \quad (13)$$

so,

$$\frac{\vartheta}{2} = \sin^{-1}\left(\frac{w}{d}\right) \quad (14)$$

and consequently,

$$\vartheta = 2\sin^{-1}\left(\frac{w}{d}\right) \quad (15)$$

The area is given by:

$$As' = \frac{1}{2}r^2(\vartheta - \sin\vartheta) \quad (16)$$

Substituting Eq. (15) into Eq. (16), we get:

$$As' = \frac{1}{2}r^2\left[2\sin^{-1}\left(\frac{w}{d}\right) - \sin\left(2\sin^{-1}\left(\frac{w}{d}\right)\right)\right] \quad (17)$$

hence,

$$2As' = \frac{d^2}{4}\left[2\sin^{-1}\left(\frac{w}{d}\right) - \sin\left(2\sin^{-1}\left(\frac{w}{d}\right)\right)\right] \quad (18)$$

To find the rectangular area equation, Eq. (12) and Eq. (18) are subtracted from the area of the circle (*Ac*):

$$Arec = Ac - 2As - 2As' \quad (19)$$

Hence, substituting (7), (12),(18) and in equation (19), we get the following equation:

$$Arec. = \frac{d^2}{4}\left[\pi - 2\cos^{-1}\left(\frac{w}{d}\right) + \sin\left(2\cos^{-1}\left(\frac{w}{d}\right)\right)\right] - \left[2\sin^{-1}\left(\frac{w}{d}\right) - \sin\left(2\sin^{-1}\left(\frac{w}{d}\right)\right)\right] \quad (20)$$

And

$$Arec. = \frac{d^2}{4}\left[\pi + \sin\left(2\sin^{-1}\left(\frac{w}{d}\right)\right) + \sin\left(2\cos^{-1}\left(\frac{w}{d}\right)\right) - 2\sin^{-1}\left(\frac{w}{d}\right) - 2\cos^{-1}\left(\frac{w}{d}\right)\right] \quad (21)$$

By determining the width (w) and the centre of the image, and applying it to equation (21), the ROC can be extracted easily and accurately as shown in Fig. 5.

This area will be identified as ROC. The ROC consists of two regions, as shown in Fig. 6, namely:
1- Region of Interest (ROI);
2- Background Region of Interest (B-ROI).

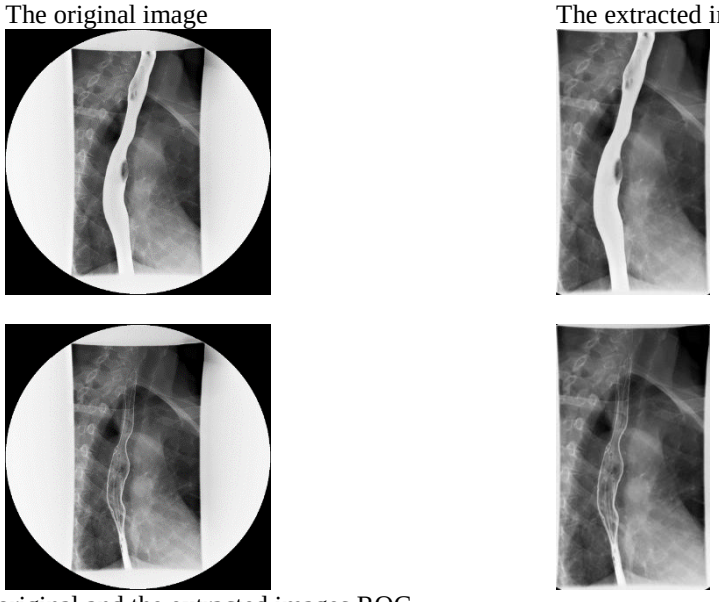

Fig. 5: The original and the extracted images ROC.

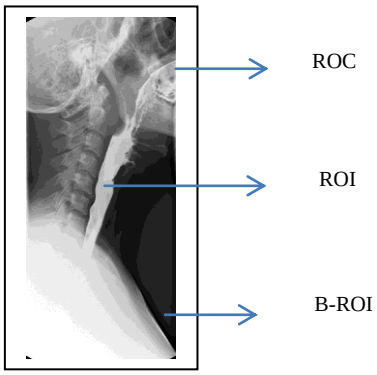

Fig. 6: Important areas in ROC Fluoroscopy images.

B-3 Extract the ROI:

In this work where the ROI is the esophagus and pharynx, there is only one part of the image that needs to be compressed losslessly. This area would need to be segmented and extracted, as in Fig. 7 (b). The steps involved are:

B-3-1 Histogram analysis to determine the peaks in the image (see Fig. 8 (b)).

B-3-2 Thresholding based on the peaks in the histogram (see Fig. 8 (c) for threshold image).

B-3-3 Calculating the areas inside the image to determine the pharynx and the esophagus areas.

B-3-4 Generate an ROI mask.

B-3-5 Applying a median filter and the morphological erosion technique to smoothen the mask.

B-3-6 Segment the threshold image (see Fig. 8 (d)).

B-3-7 Classification of the esophagus based on shape and size. Fig. 8 (e) shows the ROI image.

B-3-8 Cropping unnecessary area surrounding ROI part. Fig.8 (f) shows the cropped ROI.

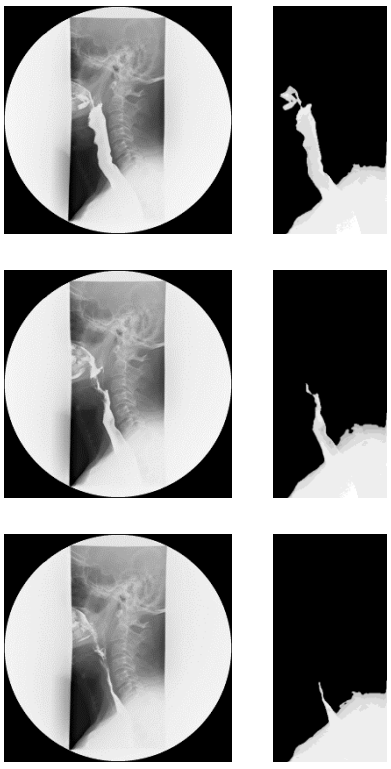

(a) Original Images (b) Segmented Images

Fig. 7: Set of Pharynx and Esophagus Fluoroscopy images taken from the same view.

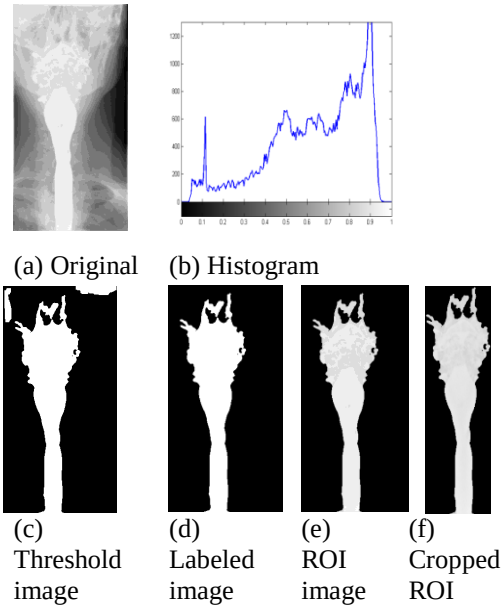

Fig. 8: ROI extraction steps.

B-4 Compute the image difference:

Calculate the difference between images by subtracting the second image (test image) from the first image (reference image), as most images taken from the same angle are mostly comparable. Therefore, we can use the first image (reference image) as the base pattern and store only the variance results as a vector (see Fig. 9).

***B.5* Encoding:**

The segmentation (stage B) produces a one dimensional vector. Depending on the construction of the vector data, we can determine the method of coding. The combination of Run-length and Huffman coding is selected because they are based on duplication and the estimated probability of appearance for each possible value of the source symbol (see Fig. 10).

RESULTS AND DISCUSSION

Experiments were performed on 57 gray scale stillclinical fluoroscopy images obtained from the Serdang Hospital, Malaysia to evaluate the validity of the proposed approach. Each image was of dimension 512×512 pixels and file size of 256KB. The performance evaluation, in terms of Compression Ratio (CR), is tabulated in Table 1. The CR is calculated as follows:

$$\mathrm{CR} = \frac{S_o}{S_d} \qquad (22)$$

where

S_o = File size of the original image,

S_d = File size of the difference image.

Table 1 shows the correlation values between the reference and the tested images for a random sample of eight images. The higher correlation corresponds to a higher similarity, resulting in a higher CR. From Table 1, it is also observed that the proposed method (R. Huff-Crop.) achieved significantly better performance than implementing Run-length Huffman Segmented (R. Huff-Seg.) on the difference images and it also performed better than the standard lossless combination (R. Huff-S) compression of the images. For example, in the case of images 005 and 006, the standard combination method (R. Huff-S) only produced a CR of 1.38. Run-length Huffman coding (R. Huff) for the difference images realized a CR of 11.41 while (R. Huff-Seg.) for the ROI difference images achieved a CR of 12.21. However, the proposed method (R.Huff-Crop.) implemented based on the CC indications, achieved a CR of 34.04 for the cropped ROI difference image (005-006).

To validate the quality of performance of the proposed framework for image compression, the error between the original image and decompressed image was calculated using MSE (Mean Square Error). The results obtained were a perfect match of zero error, proving that the developed technique is lossless.

Conclusion:

In this paper, a new framework for lossless image compression for groups of the images based on the correlation has been proposed. The technique concentrates on the ROI to code the difference between the groups of images using a combination of Run-length and Huffman coding. The method has achieved significant improvement in compression performance, and indirectly benefitsin storage and transmission.

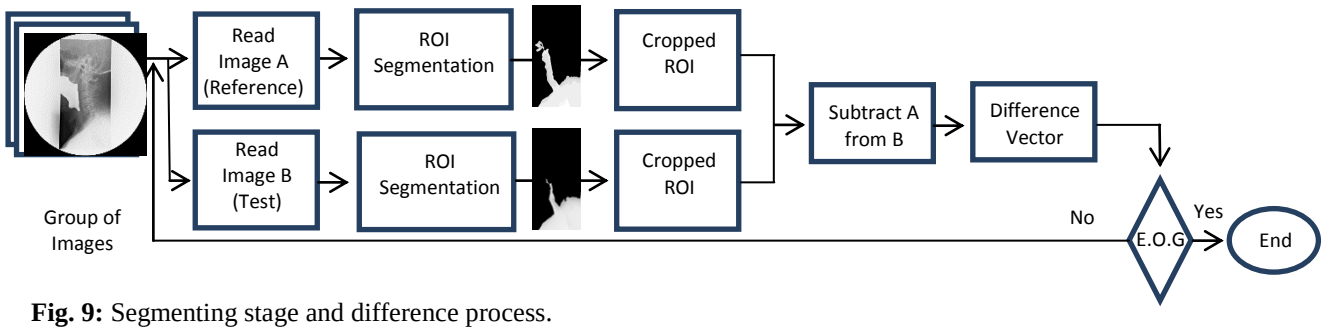

Fig. 9: Segmenting stage and difference process.

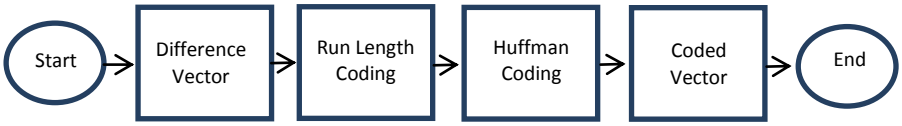

Fig. 10: Encoding stage.

Table 1: Comparison of compression ratio performance (CR) between the proposed method the combination of Run-length and Huffman coding (R. Huff-Seg.) on the difference segmented images as compared to the implementation of the combination of Run-length and Huffman coding on the difference images (R. Huff) and to the combination of Run- length and Huffman coding (R. Huff-S) on the standard image for a random sample of ten images.

Ref Image	Test Image	CC*	Compression Ratio (CR)			
			R. Huff	R. Huff (Diff)	R. Huff–ROI.	R. Huff-Cropped ROI
330005	330006	0.93	1.38	11.41	12.21	34.04
330004	330005	0.95	1.34	11.20	14.82	39.63
330009	330010	0.95	1.36	11.04	13.83	41.64
330007	330008	0.95	1.36	10.55	12.88	47.54
330010	330011	0.95	1.35	9.81	12.83	48.96
330006	330007	0.95	1.36	10.79	16.51	50.67
330012	330013	0.98	1.35	10.57	20.89	52.10
330013	330014	0.98	1.35	9.49	23.88	58.23
011004	011005	0.86	1.33	5.91	9.29	12.67
011008	011009	0.94	1.32	5.88	9.27	13.72
011005	011006	0.88	1.33	5.73	7.32	15.84
011012	011013	0.98	1.35	6.84	13.36	16.33
011011	011012	0.95	1.37	7.11	15.54	19.52
011006	011007	0.95	1.34	6.64	14.77	24.04
011007	011008	0.97	1.35	6.87	16.25	35.13
011010	011011	0.99	1.31	6.96	29.73	37.32
011013	011014	0.97	1.36	6.8	15.41	46.38

Table 2: Comparison of average compression ratio performance (ACR) between the proposed method the combination of Run-length and Huffman coding (R. Huff-Seg.) on the difference segmented images as compared to the implementation of the combination of Run-length and Huffman coding on the difference images (R. Huff) and to the combination of Run Length and Huffman coding (R. Huff-S) on the standard image for a random sample of ten images.

Group No.	No. of Images	Average of Compression Ratio (ACR)			
		R. Huff	R. Huff (Diff)	R. Huff-ROI.	R. Huff-Cropped ROI
011	13	1.35	8.22	16.15	45.51
330	19	1.31	9.85	18.83	76.38
954	25	1.34	5.85	18.76	60.59

ACKNOWLEDGEMENT

The authors would like to thank Dr. Sharifah Mastura Syed Abu Bakar (Head, Radiology Department), Khatijah Ali (Radiographer) and Ang Kim Liong (Clinical Research Centre) at Serdang Hospital, Malaysia, for their assistance and collaboration in undertaking this work. The authors would also like extend their gratitude to the group of medical experts, namely, Dr. Noraini Abd Rahim (Consultant Radiologist / Head Radiology Department), Dr. Shalini Rajandran Nair (Radiologist) and Dr. Noor Najwa Paiman (Medical Officer) at the National Cancer Institute, Malaysia, for their assistance in evaluating the reconstructed images and collaboration undertaken in this work.

REFERENCES

Akhtar, P., M. Bhatti, T. Ali, M. Muqeet, 2007. Significance of region of interest applied on MRI image. IEEE 1st International Conference on Tele Radiology-Telemedicine, Bioinformatics and Biomedical Engineering, pp: 1331-1334.

Arif, A., S. Mansor, R. Logeswaran, H. Abdul Karim, 2012. Lossless compression of fluoroscopy

medical images using correlation. Journal of Asian Scientific Research, 11(2): 718-723.

Arif, A., S. Mansor, R. Logeswaran, H. Abdul Karim, 2012. Lossless compression of fluoroscopy medical images using correlation and the combination of Run Length and Huffman coding. IEEE International Conference on Biomedical Engineering& Science(IECBES), pp: 759-762.

Bairagi, V., A. Sapkal, 2012. Automated region-based hybrid compression for digital imaging and communications in medicine magnetic resonance imaging images for telemedicine applications. IET Science, Measurment & Technology, 6(4): 247- 253.

Bharti, P., S. Gupta, R. Bhatia, 2009. Comparative analysis of image compression techniques acase study on medical images.IEEE International Conference on Advances in Recent Technologies in Communication and Computing, Kottayam, Kerala, pp: 820-822.

Choong, M., R. Logeswaran, M. Bister, 2006. Improving Diagnostic Quality of MR Images Through Controlled Lossy Compression using SPIHT. Journal of Medical Systems, 30(3): 139-143.

Doukas, C., I. Maglogiannis, 2007. Region of interest coding techniques for medical image compression. IEEE Engineering in Medicine and Biology Magazine, 26(5): 29-35.

Javed, M., M. Khan, 2008. Wavelet based medical image compression through prediction. IEEE International Multi Topic Conference, Karachi, pp: 155-159.

Kumar, N., C. Kamargaonkar, 2013. A survey on various medical image compression techniques. International Journal of Science, Engineering and Technology Research, 2(2): 501-506.

Kumar, R., S. Koliwad, G. Dawrakish, 2008. Lossless compression of digital mammography using fixed block segmentation and pixel grouping. IEEE 6th Indian Conference on Computer Vision, Graphics & Image Processing, Bhubaneswar, pp: 201-206.

Mei-Yen, C., L. Chien-Tsai, S. Ying-Chou, *et al*: 2007. Design and evaluation of a DICOM compliant video fluoroscopy imaging system. In: Proceeding of IEEE9th International Conference on Health Networking Application and Services, Taipei, pp: 248-251.

Norani, M., M. Tehranipour, 2005. RL-Huffman encoding for test compression and power reduction in scan applications. ACM. Transactions, 10(1): 91-115.

Novoa, F., A. Curra, M. Lopez, 2011. Angiographic images segmentation techniques. In: Information Recourses Management Association, Ideal Group Inc.(IGI), pp: 368-376.

Nu´n˜ez, J., S. Jones, 2003. Run-length coding extensions for high performance hardware data compression.IEE Proceeding Computer Digital Techniques, 150(6): 387-395.

Ramesh, S., 2010. Medical Image Compression using Wavelet Decomposition for Prediction Method. International Journal of Computer Science and Information Security, 7(1): 262-265.

Russakoff, D., T. Rohlfing, C. Maurer, 2002. Fuzzy segmentation of X-ray fluoroscopy images. In: Proceedings of SPIE, 4684: 146-154.

Sameh, A., S. Mansor, R. Logeswaran, H. Abdul Karim, 2013. Segmentation and compression of pharynx and esophagus fluoroscopic images. IEEE International Conference on Signal and Image Processing Applications (ICSIPA).

Setia, V., V. Kumar, 2012. Coding of DWT coefficients using Run-length coding and Huffman coding for the purpose of color image compression.International Journal of Computer and Communication Engineering, 6: 201-204.

Song, T., T. Shimamoto, 2007. Reference Frame Data Compression Method for H.264/AVC. IEICE Electronics Express, 4(3): 121-126.

Sunder, R., C. Eswaran, N. Sriraam, 2005. Performance evaluation of 3-D transforms for medical image compression. IEEE International Conference, Electro Information Technology, 6: 6.

Ukrit, M., A. Umamageswari, G. Suresh, 2011. A survey on Lossless Compression for Medical Images.International Journal of Computer Applications, 31(8): 47-50.

V˘aduva, C., T. Cost˘achioiu, C. P˘atra¸scu, I. Gav˘at, 2013. A Latent Analysis of Earth Surface Dynamic Evolution Using Change Map Time Series. IEEE Transactionon Geoscienceand Remote Sensing, 51(4): 2105-2118.

Zhang, Q., H. Xiao, 2008. Extracting regions of interests in biomedical images. IEEE International Seminar on Future Biomedical Information Engineering, pp: 3-6.